Journal of Power Sources 195 (2010) 744–749

Contents lists available at ScienceDirect

Journal of Power Sources

journal homepage: www.elsevier.com/locate/jpowsour

# A new anode material for solid oxide electrolyser: The neodymium nickelate $Nd_2NiO_{4+\delta}$

F. Chauveau[a], J. Mougin[b], J.M. Bassat[a], F. Mauvy[a], J.C. Grenier[a,*]

[a] CNRS, Université de Bordeaux, ICMCB, 87 avenue du Dr. A. Schweitzer, Pessac, F-33608, France
[b] CEA-Grenoble, LITEN/DTH, 17 rue des Martyrs, F-38054 Grenoble Cedex 9, France

ARTICLE INFO

*Article history:*
Received 30 April 2009
Received in revised form 29 July 2009
Accepted 3 August 2009
Available online 12 August 2009

*Keywords:*
Solid oxide electrolysis cell (SOEC)
High temperature steam electrolysis (HTSE)
Anode material
Oxygen electrode
Nickelate oxide
Impedance spectroscopy

ABSTRACT

Neodymium nickelate, with composition $Nd_2NiO_{4+\delta}$ is integrated as oxygen electrode in a solid oxide electrolyte supported cell made of a TZ3Y electrolyte and a Ni-CGO hydrogen electrode. This cell is tested in both fuel cell (SOFC) and electrolysis (SOEC) mode and the reversible operation is proven, ASR values being slightly lower in electrolysis mode. Performances in SOEC mode are compared with a commercial cell based on the same electrolyte and cathode, but with lanthanum strontium manganite (LSM) as anode. For a voltage of 1.3 V, current densities of 0.40, 0.64 and 0.87 A $cm^{-2}$ are measured at 750, 800 and 850 °C, respectively; they are much higher than the ones measured in the same conditions for the LSM-containing cell. Indeed, for a voltage of 1.3 V, current densities are respectively 1.7, 3 and 4.2 times higher for the $Nd_2NiO_{4+\delta}$ cell than for the LSM one at 850, 800 and 750 °C, respectively. Consequently, $Nd_2NiO_{4+\delta}$ can be considered as a good candidate for operating below 800 °C as oxygen electrode for high temperature steam electrolysis.



## 1. Introduction

For economical and ecological reasons, hydrogen is considered as a major energetic vector for the future. In order to gain the status of leading alternative fuel, one major question which still remains to be solved, is the massive production using clean processes with low or no $CO_2$ emissions. High temperature steam electrolysis (HTSE) is one of the most promising processes to achieve this target, water molecule being split into hydrogen and oxygen using electricity and heat which can be provided by nuclear power plants for example [1]. However, in order to produce by HTSE the amount of hydrogen needed to replace even partially the fossil fuels, many dedicated power plants would be necessary. Thus, the development of highly efficient systems is required. Each component of the system has to be optimized, from the balance of plant to the solid oxide electrolysis cell (SOEC) where the HTSE reaction occurs. Most of current studies reported on HTSE consider reversible solid oxide cells (fuel cell/electrolysis cell) [2–5], containing hydrogen electrode made of cermet, zirconia based electrolyte, and perovskite-type oxygen electrode. An alternative oxygen electrode material, whose composition is $Nd_2NiO_{4+\delta}$, is presented in this work.

The $Ln_2NiO_{4+\delta}$-type oxides (with the $K_2NiF_4$-type structure) have been selected because of their aptitude to accommodate a large oxygen overstoichiometry, especially under oxidizing conditions [6], this capability leading to a mixed electronic and ionic conductivity of these materials. This explains the strong interest in these compounds as solid oxide fuel cell (SOFC) cathode material [7]. Recently it was reported that, under anodic polarization, $La_2NiO_{4+\delta}$ oxide exhibits a lower polarization resistance than under cathodic polarization [8]. The $Nd_2NiO_{4+\delta}$ oxide was selected for this study because of its higher overstoichiometry compared to the other $Ln_2NiO_{4+\delta}$-type oxides [9], which should lead to further improved performances.

Results on performances of this material in SOEC mode are reported here in comparison with the classical LSM (lanthanum strontium manganite) perovskite oxygen electrode. Polarization ($i$–$V$) curves are presented at different temperatures on single cells and discussed in combination with corresponding electrochemical impedance spectroscopy (EIS) measurements. Thanks to the use of a specific setup containing a reference electrode, anodic and cathodic contributions are separated and discussed.

## 2. Experimental

### 2.1. Description of the cell

The single solid oxide cell (SOC) concerned with this work is a planar electrolyte supported cell. The electrolyte has a 50 mm

* Corresponding author. Tel.: +33 5 40 00 62 62; fax: +33 5 40 00 27 61.
*E-mail address:* grenier@icmcb-bordeaux.cnrs.fr (J.C. Grenier).

0378-7753/$ – see front matter © 2009 Published by Elsevier B.V.
doi:10.1016/j.jpowsour.2009.08.003

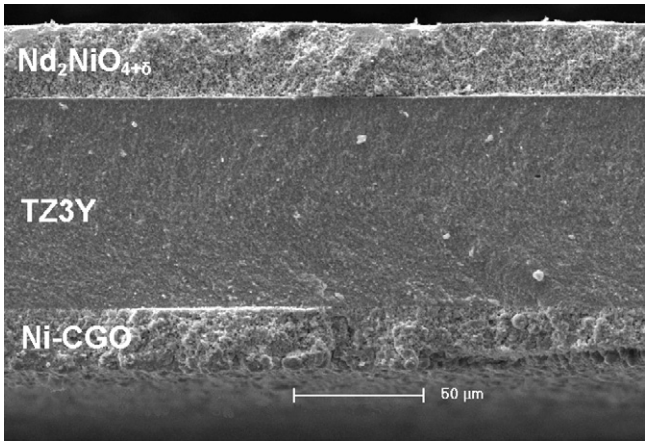


**Fig. 1.** SEM micrograph of the cell cross-section after electrochemical measurements.

diameter and both electrodes have a 20 mm diameter, which corresponds to a 3.14 $cm^2$ active surface area. The oxygen electrode ($Nd_2NiO_{4+\delta}$) was manufactured at ICMCB and deposited on half cells composed of electrolyte and hydrogen electrode provided by H.C. Starck Ceramics GmbH & Co. KG [10].

The electrolyte is a 90 μm thick substrate of 3% tetragonal yttria stabilized zirconia (TZ3Y) and the hydrogen electrode is a 30 μm thick porous nickel and gadolinia doped ceria cermet (Ni-CGO).

The $Nd_2NiO_{4+\delta}$ powder was prepared by the nitrate–citrate route as described by Courty et al. [11]. Stoichiometric amounts of neodymium and nickel oxides were dissolved in diluted nitric acid. After addition of a large excess of citric acid for chelating the cations, the solution was dehydrated and heated until self-combustion of the precipitate to obtain submicronic precursor particles [9]. The final annealing was performed at 1000 °C for 12 h to obtain a single phase. The powder was then ball milled to obtain an median grain size ($d_{0.5}$) of about 0.8 μm. A terpineol-based slurry was prepared with this powder, and then deposited on the electrolyte by screen printing before a sintering step at 1100 °C for 3 h in air [12]. The thickness of the final $Nd_2NiO_{4+\delta}$ porous layer was about 30 μm (Fig. 1).

A gold annular reference electrode (2 mm wide) was painted on the oxygen electrode side of the electrolyte and then annealed at 750 °C for 30 min in air (Fig. 2). The distance between working and reference electrodes (more than 100 times the thickness of the electrolyte) was set to avoid as much as possible measurement artifacts due to the influence of the current lines through the electrolyte on the reference electrode [13]. The studied cell was placed in a ceramic housing and sealed using glass paste and gold rings, the whole being inside a specific setup equipped with a so-called 3rd chamber with controlled atmosphere for the reference electrode (Fig. 2). The pressure in each chamber was 1 atm. Before

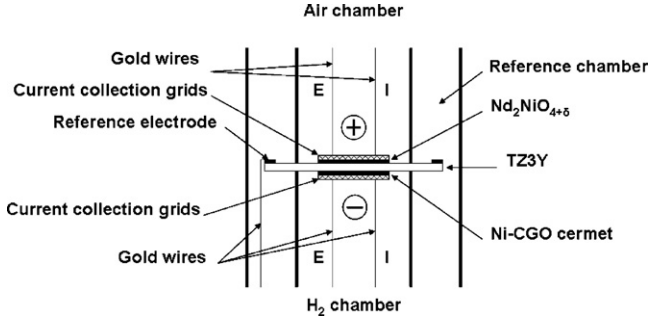


**Fig. 2.** Schematic representation of the test rig.

electrochemical measurements, the hydrogen electrode provided under NiO-CGO form was reduced at 750 °C in an $Ar/H_2$ mixture with increasing amounts of hydrogen, up to 100%.

With the aim of comparing, a commercial electrolyte supported cell provided by H.C. Starck Ceramics GmbH & Co. KG under the commercial name ESC2 was also tested in the same conditions. Electrolyte and hydrogen electrode were identical as described above, while the oxygen electrode was a double layer made of pure LSM and 8YSZ (8% yttria stabilized zirconia)/LSM, with a total thickness around 30–50 μm.

### 2.2. Electrochemical measurements

The inlet gas composition at the hydrogen electrode was composed of hydrogen (4 L $h^{-1}$), water vapor (3.7 L $h^{-1}$) and argon (3 L $h^{-1}$). This amount of water vapor was obtained by total evaporation of liquid water (3 mL $h^{-1}$). All the measurements reported hereafter were recorded for a ratio $p(H_2O)/p(H_2) = 0.9$. The inlet gas to the $Nd_2NiO_{4+\delta}$ side was air (7 L $h^{-1}$), the reference electrode compartment was under an argon flow in order to fix a constant oxygen partial pressure at the reference electrode. Current collectors on both positive and negative electrodes were gold grids (1024 meshes $cm^{-2}$) and platinum grids (3600 meshes $cm^{-2}$), platinum grid being directly in contact to the electrodes. This assembly aims to get a good contact with ceramic electrodes. Measurements were performed at 750 °C, 800 °C and 850 °C, from the lowest to the highest temperature. *i–V* curves were recorded first in SOFC mode, then in SOEC mode. Measurements were recorded from open circuit cell voltage (OCV) to the highest polarization, then back to OCV.

The current–voltage curves were obtained by applying a dc current during 180 s for each step and recording the voltage after stabilization. These data were recorded using a power supplier (TTi QL355P 15V-5A) under galvanostatic control. The EIS measurements were also performed under galvanostatic control with a 100 mA modulation amplitude, from $10^4$ to $10^{-1}$ Hz, using an Autolab PGSTAT 302N equipped with a frequency response analyzer (FRA).

The ratio of steam-to-hydrogen conversion is calculated as the molar amount of hydrogen produced (according to the Faraday's law and assuming 100% of current efficiency) divided by the molar amount of water in the inlet cathodic gas. Cell performances are evaluated through the area specific resistance (ASR) values determined at 0.7 V in SOFC mode and at 1.3 V in SOEC mode. ASRs are calculated as the slopes of *i–V* curves between 0.65 and 0.75 V for SOFC mode, and between 1.25 and 1.35 V in SOEC mode.

*i–V* curves and impedance diagrams were recorded on complete cell on one hand (between anode and cathode), and on the other hand using the reference electrode, that is to say between anode and reference or between cathode and reference to separate the anode and cathode contributions to the global signal.

## 3. Results and discussion

### 3.1. Cell performances

Current–voltage curves given in Fig. 3, for the three temperatures, were recorded first in fuel cell mode, then in electrolysis one, starting from OCV in each case. These results show that cell can be operated both in SOFC and SOEC modes in agreement with previous studies [2,4]. One should note that the measured OCVs are somewhat smaller than the theoretical Nernst potentials, typically at 800 °C, 0.86 V instead of 0.95 V, which reflects the presence of a slight leak in the setup.

Plots in fuel cell mode are quite linear, highlighting the absence of activation. In electrolysis mode, curves are inflecting, likely reflecting an activation phenomenon. No limiting current

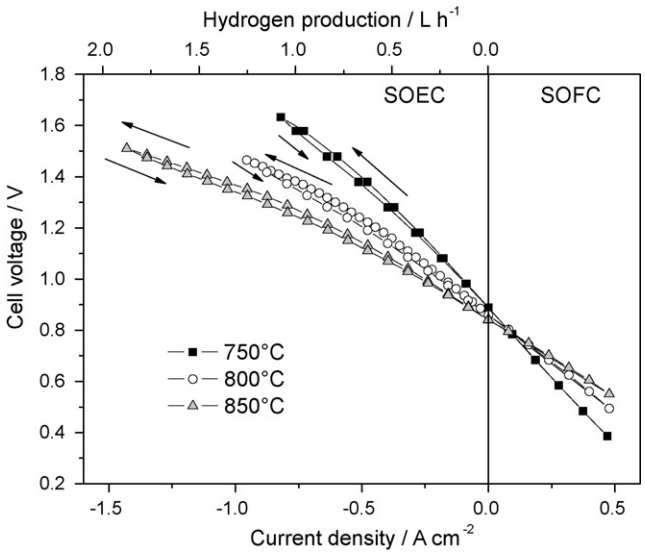


**Fig. 3.** Current density–voltage curves at various temperatures; the ratio $H_2O/H_2$ is 0.9 at the hydrogen electrode; the corresponding hydrogen production is given on the upper axis.

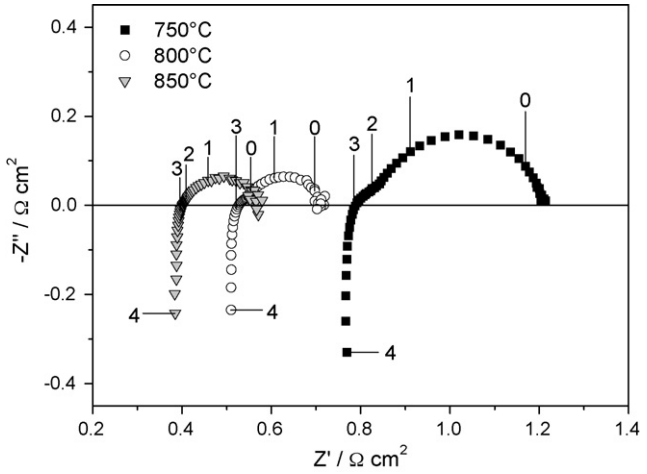


**Fig. 4.** Cell impedance diagrams recorded at open circuit voltage at various temperatures. Frequency logarithms are given on the plots.

is observed whatever the temperature, on the contrary to results reported by Hauch et al. [2] and Brisse et al. [4] for similar steam-to-hydrogen conversion and absolute humidity values, but for different types of cells.

In addition, *i–V* measurements in SOEC mode show a slight hysteresis effect which is not observed in SOFC mode. Hauch et al. also reported a hysteresis effect in SOEC mode [2], but in the opposite way of ours. The origin of this hysteresis loop is not yet explained. It may be due to a Joule heating effect when increasing the current density, which could raise the temperature and then increase the conductivity of the different cell components. However, this possibly heating effect has not been evidenced through the thermocouples located close to the cell in the test rig.

For a voltage of 1.3 V, current densities of 0.40, 0.64 and 0.87 A cm$^{-2}$ have been measured at 750, 800 and 850 °C, respectively, on the decreasing current curve. They corresponded to a percentage of steam-to-hydrogen conversion of 14, 23 and 31% with respect to the experimental conditions of this study. ASR values of the complete cell measured in SOEC mode (at 1.3 V) are lower than the ones measured in SOFC mode (at 0.7 V) as shown in Table 1, reflecting the slope inflection observed in SOEC mode. This decrease in ASR may have several origins. For instance, one can assume that under anodic polarization, the nickelate is likely to be oxidized. Then, the amount of $Ni^{3+}$, *i.e.* the hole concentration, increases, which would induce an increase of the electrical conductivity as well as of the electrocatalytic properties. However, we do not have evidence of this oxidation (experiments are in progress). Another reason could be the increase of the sample temperature resulting from high values of the current density as previously quoted.

Nyquist diagrams of the EIS measurements recorded at OCV for the three studied temperatures are given in Fig. 4. The general features of the diagrams and their frequency distribution are similar for the three temperatures, showing that the electrochemical processes remain unchanged for the considered temperature range. Total resistances taken as the diagram intercepts with real axis at low frequencies are equal to 1.20, 0.71 and 0.57 Ω cm$^2$ at 750, 800 and 850 °C, respectively. They are consistent with ASR values calculated from *i–V* curves and given in Table 1. Moreover, it can be seen that the cell polarization resistance decreases with increasing temperature, indicating that electrochemical processes are thermally activated for both electrodes.

### 3.2. Anode and cathode contributions

In this section, only the electrolysis mode will be considered; the $Nd_2NiO_{4+\delta}$ electrode will be called "anode" and the Ni-CGO electrode, "cathode". The aim of this part is to deconvoluate the anodic and cathodic contributions in the global signal recorded on *i–V* curves shown in Fig. 3. Indeed, the voltage measured in the two electrodes configuration is composed of different voltage losses according to Eq. (1).

$$E_{cell} = E_{Nernst} + |R \times I| + |\eta(\text{Ni-CGO})| + |\eta(Nd_2NiO_{4+\delta})| \quad (1)$$

$E_{Nernst}$ is the potential resulting from the oxygen partial pressure difference between the air and the hydrogen chambers, the $R \times I$ term is the voltage loss due to the ohmic resistance related to the current flow through the cell and the two final terms represent the overpotentials $\eta$ of both electrodes. *i–V* curves between anode and reference and between cathode and reference were recorded. They are plotted in Fig. 5 for the temperature of 750 °C and compared to the *i–V* curve measured on the complete cell (two electrodes measurements, between anode and cathode). The sum of $Nd_2NiO_{4+\delta}$/reference voltage (anodic contribution) and Ni-CGO/reference voltage (cathodic contribution) gives the same value as the one measured between $Nd_2NiO_{4+\delta}$ and Ni-CGO electrodes. It is clearly evidenced in Fig. 5, which confirms the reference electrode

**Table 1**
Area specific resistances determined from data plotted in Fig. 3 as a function of temperature in both SOFC mode (at 0.7 V) and in SOEC mode (at 1.3 V).

| Temperature (°C) | ASR (Ω cm$^2$) | | | |
|---|---|---|---|---|
| | SOFC (0.7 V) | OCV | SOEC (1.3 V) | |
| | | | Increasing current | Decreasing current |
| 750 | 1.09 | 1.09 | 0.96 | 0.89 |
| 800 | 0.74 | 0.74 | 0.58 | 0.55 |
| 850 | 0.60 | 0.60 | 0.43 | 0.39 |

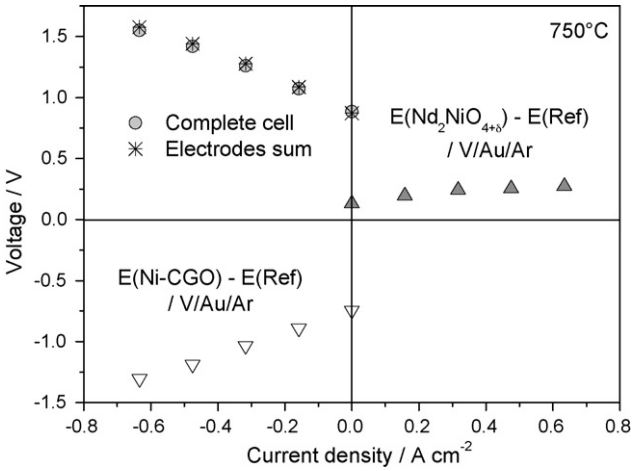


**Fig. 5.** Current density–voltage curves recorded in the electrolysis mode at 750 °C, between the oxygen electrode ($Nd_2NiO_{4+\delta}$) and the reference (▲), between the hydrogen electrode (Ni-CGO) and the reference (▽), then compared with the measurements between the oxygen and hydrogen electrodes (●); stars symbols correspond to the sum of voltages of the first two contributions; reference electrode flushed with argon. By convention, the cathodic reaction corresponding to a reduction is plotted with a negative current density whereas the anodic reaction corresponding to an oxidation is plotted with a positive current density.

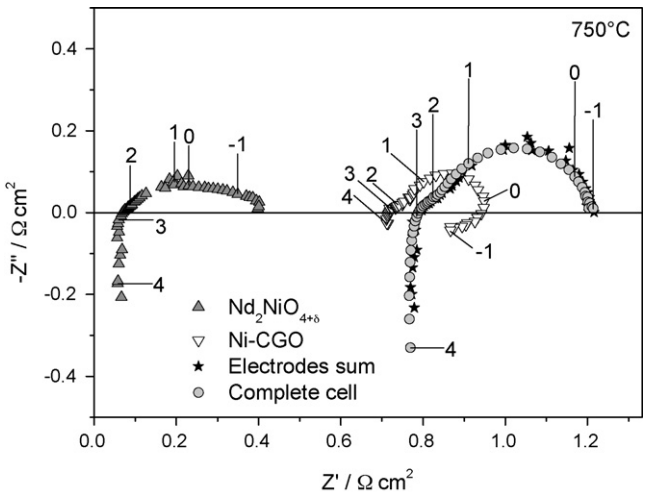


**Fig. 6.** Impedance diagrams recorded at 750 °C at open circuit voltage between the oxygen electrode and the reference (▲), between the hydrogen electrode and the reference (▽) and between the oxygen and hydrogen electrodes (●) under controlled gas composition in the reference chamber. The stars represent the vectorial sum of the two first contributions. Frequency logarithms are given on the plots.

to be stable under polarization. The slope measured on the anodic *i–V* curve is smaller than the one measured on the cathodic one. Indeed, ASR values at 1.3 V are equal to 0.18 Ω cm² for $Nd_2NiO_{4+\delta}$ and to 0.83 Ω cm² for Ni-CGO. Nevertheless, as for the complete cell, the voltages measured with the reference electrode are composed of different voltage losses according to Eqs. (2) and (3).

$$E(Nd_2NiO_{4+\delta}) - E(\text{ref}) = E^{a}_{\text{Nernst}} + \left|R^{a} \times I\right| + \left|\eta(Nd_2NiO_{4+\delta})\right| \quad (2)$$

$$E(\text{Ni} - \text{CGO}) - E(\text{ref}) = E^{c}_{\text{Nernst}} - \left|R^{c} \times I\right| - \left|\eta(\text{Ni} - \text{CGO})\right| \quad (3)$$

In these equations, $E^{a}_{\text{Nernst}}$ and $E^{c}_{\text{Nernst}}$ correspond to the voltage due to the oxygen partial pressure difference between the different chambers (air/reference chambers and hydrogen/reference chambers respectively, a meaning anode and c meaning cathode). The sum of $R^{a}$ and $R^{c}$ is the complete cell ohmic resistance $R$ presented in Eq. (1). The ASR values measured on the $Nd_2NiO_{4+\delta}$/reference and the Ni-CGO/reference *i–V* curves correspond to the sum of the polarization resistance of each electrode and the ohmic losses. Impedance spectroscopy measurements have been performed on the complete cell on one hand and on anode/reference and cathode/reference on the other hand. Diagrams recorded at OCV for these three configurations at 750 °C are given in Fig. 6. As for the *i–V* curves, the sum of diagrams recorded on anodic and cathodic sides (vector sum for each frequency) fit perfectly to the experimental diagram recorded between anode and cathode. Global ASR may be divided into ohmic resistance (*R*s) and electrode polarization resistance (*R*p). The ohmic resistance originates from the electrolyte, the electrode materials and the current collection arrangement. Ohmic losses are taken as the intercept of the diagram with the $Z'$ axis at high frequencies; on the other hand, the polarization resistance of the electrodes can be determined by subtracting the previous ohmic contribution to the total resistance obtained from the intercept with the $Z'$ axis at low frequencies. Fig. 6 shows that the ohmic resistance is equal to 0.79 Ω cm² for the complete cell. For an electrolyte thickness of 90 μm, measured on SEM micrograph (Fig. 1), the electrolyte resistance has been determined and is equal to 0.75 Ω cm². It means that the contribution of other resistances is very small, about 0.04 Ω cm², in agreement with the use of gold and platinum fine mesh grids as described in Section 2.2.

Anodic ($Nd_2NiO_{4+\delta}$/reference) and cathodic (Ni-CGO/reference) impedance diagrams exhibit large differences in terms of ohmic resistance, the value being much higher for the cathodic diagram (0.72 Ω cm²) than for the anodic one (0.07 Ω cm²). As the resistance due to current collection can be considered as almost zero, it can be asserted that ohmic resistances represent mainly electrolyte contribution. Since ohmic resistances measured on the anode side are small when compared to the cathode side, it means that the electrolyte contribution is not equally distributed between the two sides of the cell, suggesting that the equipotential lines are disturbed and deviated close to the $Nd_2NiO_{4+\delta}$ electrode. This feature might be due to the very small thickness of the electrolyte and consequently to the very small distance between both electrodes, which likely distorts the current and potential lines distribution in between as previously observed by Adler et al. [13].

As consequence, electrolyte contributes with a ratio of 91% for the cathodic diagram and *i–V* curve, and only for 9% for the anodic diagram and *i–V* curve at 750 °C. This trend is also observed at 800 and 850 °C, even if the ratios are slightly modified.

It can also be noticed from the diagrams in Fig. 6 that the distortions occur at low frequencies when measurements are carried out using the reference electrode. It is particularly obvious on the Ni-CGO/reference diagram, with a part of it including positive $Z''$ values at low frequencies. Since the sum of anodic and cathodic diagrams corresponds almost perfectly to the diagram recorded on the complete cell (see above), it means that if the Ni-CGO/reference diagram is distorted at low frequencies, the $Nd_2NiO_{4+\delta}$/reference diagram is distorted as well (and in the exact opposite way). Such inductive loop was already reported in literature [14,15] and originates from the difference of the impedance time constants of the electrodes.

Due to the distortion of the Ni-CGO/reference diagram, the determination of the electrode polarization resistance cannot be simply determined considering the low frequency intercept. The arc in positive $Z''$ part has to be taken into account to determine the polarization resistance. In such a way, the polarization resistance of Ni-CGO is equal to 0.1 Ω cm² and that of $Nd_2NiO_{4+\delta}$ equal to 0.35 Ω cm². The sum, equal to 0.45 Ω cm² is in very good agreement with the value measured on complete cell diagram and equal to 0.42 Ω cm². Hence the polarization resistance for $Nd_2NiO_{4+\delta}$ is 3–4 times higher than the one of Ni-CGO.

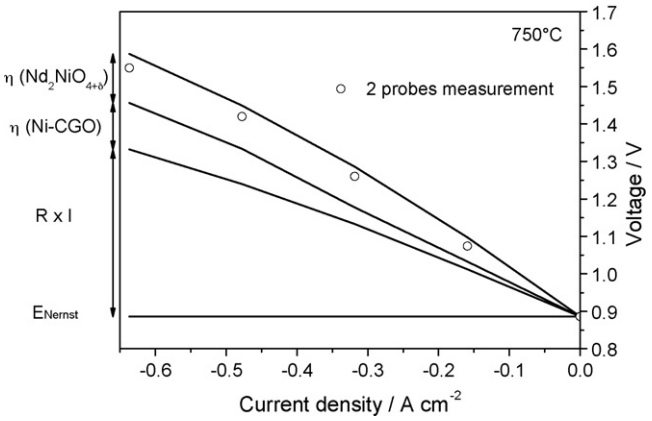


**Fig. 7.** *i–V* curve measured at 750 °C in electrolysis mode (○) and split into ohmic losses ($R \times I$) and electrodes overpotentials.

Using the same way, ohmic resistances were obtained from impedance diagrams for each electrode, and for each current density. Using also the *i–V* curves recorded between anode and reference, then between cathode and reference, the overpotentials can be deduced.

In Fig. 7 are plotted the different voltage losses in the electrolysis mode at 750 °C. The Nernst voltage is considered to be constant and measured at OCV. The ohmic losses were calculated by multiplying the current density applied to the cell by the ohmic resistance measured by impedance spectroscopy on complete cell (in two electrodes configuration). A slight decrease of this ohmic resistance was experimentally observed at increasing polarization, for both two and three electrodes measurements. This effect might be due to a local heating effect; however additional investigations are required to fully understand this phenomenon. This would explain the non-linearity of the $R \times I$ contribution versus current density as evidenced in Fig. 7. For each current density, the electrode overpotentials were calculated by subtracting the ohmic losses deduced from impedance diagrams in three probes configuration from the current–voltage curves also measured in three electrodes configuration. The sum of the different contributions agrees pretty well with the experimental *i–V* curve measured on complete cell. The difference between measured and calculated values (of about 40 mV for a current density of 640 mA cm$^{-2}$) is rather small with respect to the large number of used parameters.

A cell voltage of 1.3 V measured in two probes configuration at 750 °C corresponds to a current density of 360 mA cm$^{-2}$. At this working point, voltage losses are composed of 60% ohmic losses, 15% being the overpotential at hydrogen electrode and 25% overpotential at oxygen electrode. As for polarization resistances reported above, $Nd_2NiO_{4+\delta}$ overpotential is higher than Ni-CGO overpotential even if the ratio is not the same.

### 3.3. Comparison of cell performances with $Nd_2NiO_{4+\delta}$ or LSM oxygen electrode

The current density–voltage curves obtained in electrolysis mode with cells containing either the $Nd_2NiO_{4+\delta}$ oxygen electrode developed in this study or a LSM oxygen electrode (commercial ESC2 cell) are compared in Fig. 8 for different temperatures. Whatever the temperature, the current density obtained with the cell containing $Nd_2NiO_{4+\delta}$ is higher than the corresponding ESC2 type cell containing LSM. This result highlights the benefit on the voltage losses by using $Nd_2NiO_{4+\delta}$ as oxygen electrode material instead of LSM.

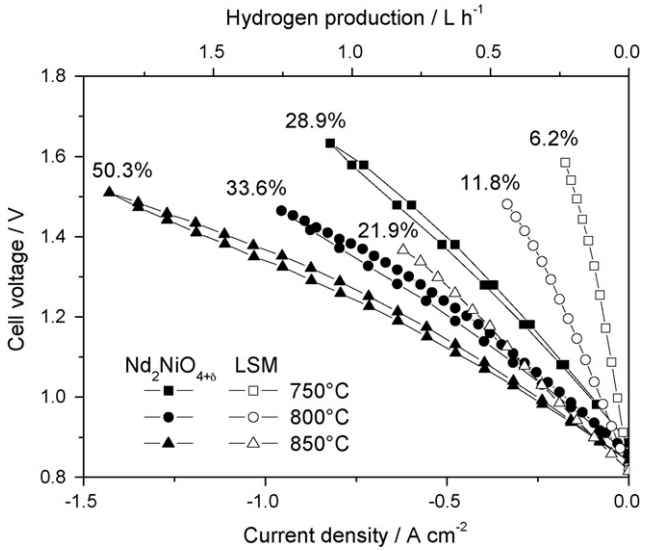


**Fig. 8.** Current density–voltage curves obtained (1) for the cell with the $Nd_2NiO_{4+\delta}$ anode (closed symbols) and (2) for an ESC2 cell with LSM anode (open symbols), at 750 °C (squares), 800 °C (circles) and 850 °C (triangles). The corresponding highest percentage of steam-to-hydrogen conversion is reported on each curve. The hydrogen production is given on the upper axis.

Fig. 8 shows that the difference in performance between $Nd_2NiO_{4+\delta}$ and LSM is more marked when temperature is decreasing. Indeed, for a voltage of 1.3 V, the current density is respectively 1.7, 3 and 4.2 times higher for the cell containing $Nd_2NiO_{4+\delta}$ with respect to the cell including LSM, at 850, 800 and 750 °C respectively. Hence, $Nd_2NiO_{4+\delta}$ seems to be particularly suitable for being used as oxygen electrode especially at temperatures below 800 °C.

In addition one can notice that the LSM oxygen electrode was optimized in a shape of a double layer using 8YSZ composite while the $Nd_2NiO_{4+\delta}$ layer was composed of a single layer without any size particles gradient as shown in the SEM micrograph of Fig. 1. In this respect, the beneficial role of $Nd_2NiO_{4+\delta}$ compared to LSM could be further increased with an optimization of the microstructure or architecture of the electrode.

## 4. Conclusions

The neodymium nickelate with composition $Nd_2NiO_{4+\delta}$ has been integrated as oxygen electrode in a solid oxide electrolyte supported cell (TZ3Y as electrolyte and Ni-CGO as hydrogen electrode). It has been tested in both fuel cell (SOFC) and electrolysis (SOEC) modes. The reversible operation of such a cell has been observed, ASR values being slightly lower in electrolysis mode for the operating conditions considered here. High performances in electrolysis mode have been obtained for the investigated temperature range, 750–850 °C. For a voltage of 1.3 V, current densities of 0.40, 0.64 and 0.87 A cm$^{-2}$ have been obtained at 750, 800 and 850 °C, respectively. The corresponding percentages of steam-to-hydrogen conversion are 14, 23 and 31% for the gas mixture considered in the present study. Such performances are better than the corresponding ones measured in the same conditions on the same type of cells but containing a LSM oxygen electrode. Indeed, for a voltage of 1.3 V, the current densities are respectively 1.7, 3 and 4.2 times higher for the $Nd_2NiO_{4+\delta}$ containing cell compared to the LSM one at 850, 800 and 750 °C, respectively. In this respect, $Nd_2NiO_{4+\delta}$ can be considered now as a good candidate for oxygen electrode of high temperature steam electrolysis operating at low temperature (below 800 °C).

Three electrodes measurements performed in conjunction with impedance spectroscopy allowed separating the anode and cathode contributions to the global cell voltage. Due to the use of an electrolyte supported cell, most of the losses are ohmic. Overpotentials as well as polarization resistances were determined for both electrodes.

## Acknowledgements

The authors wish to thank the French Research Agency (ANR) through the Hydrogen and Fuel Cells program (Pan-H) for co-financing this work in the frame of the national project SEMI-EHT (contract reference ANR-05-PANH-019).

## References

[1] R. Elder, R. Allen, Prog. Nucl. Energy 51 (2009) 500–525.
[2] A. Hauch, S.H. Jensen, S. Ramousse, M. Mogensen, J. Electrochem. Soc. 153 (9) (2006) A1741–A1747.
[3] J.S. Herring, J.E. O'Brien, C.M. Stoots, G.L. Hawkes, J.J. Hartvigsen, M. Shahnam, Int. J. Hydrogen Energy 32 (2007) 440–450.
[4] A. Brisse, J. Schefold, M. Zahid, Int. J. Hydrogen Energy 33 (2008) 5375–5382.
[5] J.R. Mawdsley, J.D. Carter, A.J. Kropf, B. Yildiz, V.A. Maroni, Int. J. Hydrogen Energy 34 (2009) 4198–4207.
[6] P. Stevens, C. Lalanne, J.M. Bassat, F. Mauvy, J.C. Grenier, France Brevet (2004), FR 2872174.
[7] H. Zhao, F. Mauvy, C. Lalanne, J.M. Bassat, S. Fourcade, J.C. Grenier, Solid State Ionics 179 (2008) 2000–2005.
[8] D. Pérez-Coll, A. Aguadero, M.J. Escudero, L. Daza, J. Power Sources 192 (2009) 2–13.
[9] E. Boehm, J.M. Bassat, P. Dordor, F. Mauvy, J.C. Grenier, P. Stevens, Solid State Ionics 176 (2005) 2717–2725.
[10] R. Huiberts, K.H. Buchner, H.P. Baldus, Proceedings of the 8th European Solid Oxide Fuel Cell Forum, Lucerne 30th June – 4th July, 2008, p. B0302.
[11] P. Courty, H. Ajot, C. Marcilly, B. Delmon, Powder Technol. 7 (1973) 21–38.
[12] C. Lalanne, G. Prosperi, J.M. Bassat, F. Mauvy, S. Fourcade, P. Stevens, M. Zahid, S. Diethelm, J. Van Herle, J.C. Grenier, J. Power Sources 185 (2008) 1218–1224.
[13] S.B. Adler, B.T. Henderson, M.A. Wilson, D.M. Taylor, R.E. Richards, Solid State Ionics 134 (2000) 35–42.
[14] S.B. Adler, J. Electrochem. Soc. 149 (5) (2002) E166–E172.
[15] M. Cimenti, V.I. Birss, J.M. Hill, Fuel Cells 5 (2007) 377–391.